Nuclear Engineering and Technology 49 (2017) 254–266

Available online at ScienceDirect

Nuclear Engineering and Technology

journal homepage: www.elsevier.com/locate/net

Original Article

Ramifications of Structural Deformations on Collapse Loads of Critically Cracked Pipe Bends Under In-Plane Bending and Internal Pressure

Sumesh Sasidharan[*], *Veerappan Arunachalam*, *and Shanmugam Subramaniam*

Department of Mechanical Engineering, National Institute of Technology, Tiruchirappalli 620 015, Tamil Nadu, India

ARTICLE INFO

Article history:
Received 6 April 2016
Received in revised form
25 August 2016
Accepted 7 September 2016
Available online 30 September 2016

Keywords:
Circumferential Through-Wall Crack
Finite-Element Analysis
Pipe Bend
Plastic Collapse Load
Structural Deformation

ABSTRACT

Finite-element analysis based on elastic–perfectly plastic material was conducted to examine the influence of structural deformations on collapse loads of circumferential through-wall critically cracked 90° pipe bends undergoing in-plane closing bending and internal pressure. The critical crack is defined for a through-wall circumferential crack at the extrados with a subtended angle below which there is no weakening effect on collapse moment of elbows subjected to in-plane closing bending. Elliptical and semioval cross sections were postulated at the bend regions and compared. Twice-elastic-slope method was utilized to obtain the collapse loads. Structural deformations, namely, ovality and thinning, were each varied from 0% to 20% in steps of 5% and the normalized internal pressure was varied from 0.2 to 0.6. Results indicate that elliptic cross sections were suitable for pipe ratios 5 and 10, whereas for pipe ratio 20, semioval cross sections gave satisfactory solutions. The effect of ovality on collapse loads is significant, although it cancelled out at a certain value of applied internal pressure. Thinning had a negligible effect on collapse loads of bends with crack geometries considered.

1. Introduction

Pipe bends and elbows in industrial piping as in the primary piping system of pressurized reactors in nuclear power plants are most often subjected to bending moment (due to dead weight or thermal shocks) and internal fluid pressure. Various researchers have utilized analytical [1–3], experimental [4–10], and numerical [11–16] methods to determine the plastic loads of pipe bends undergoing in-plane bending moment with or without internal fluid pressure. All of the aforementioned studies considered pipe bends with circular cross sections and uniform wall thickness. In an actual scenario, however, pipe bends exhibit structural deformations, namely, ovality and thinning, as an outcome of the bending processes, and the acceptance of pipe bends is based on the magnitude of these structural distortions [17–20]. The piping

* *Corresponding author.*
E-mail address: sumesh4sai@gmail.com (S. Sasidharan).
http://dx.doi.org/10.1016/j.net.2016.09.001

codes according to the American Society of Mechanical Engineers Section III recommend 8% as the maximum allowable ovality of pipe bends used for nuclear power plants. Linear and nonlinear cyclic analyses have been carried out on pipe bends with circular cross section and noncircular cross section with 8% ovality [20]. When shape imperfections are incorporated in the finite-element (FE) model, the presumed cross sections at the bend have been elliptic [17–19] and semioval [19,20]. In nuclear piping systems, pipe bends are subjected to degradation mechanisms like local wall thinning due to flow-accelerated corrosion. Kim et al. [21] had provided a method to estimate plastic loads (defined by the twice-elastic-slope) for elbows with nonuniform thicknesses under in-plane bending and under internal pressure.

Crack-like defects develop on pipe bends not only during several phases during manufacturing and installation, but also during cyclic loading and material deterioration as a consequence of continued operation [22]. A large through-wall circumferential crack could considerably lessen the load-carrying capacity of elbows [23]. Several studies on plastic limit analysis have been performed for cracked straight pipes, but only limited studies are available for cracked elbows, particularly for combined loading cases [24,25]. A detailed analysis of the mechanical behavior of pipe bends was reported [26] to explain the weakening effect caused by the presence of crack. In that study, the authors also presented limit loads solutions for pipe bends with circumferential through-wall crack under torsion moment. For circumferentially cracked elbows subjected to combined pressure and in-plane bending, published findings on plastic loads are very limited, which may be ascribed to the complexities involved in solving the problem. Chattopadhyay and Tomar [27] have provided plastic load results for circumferentially through-wall cracked elbows undergoing combined pressure and in-plane bending. They also reported that for circumferential through-wall cracks at the extrados of the pipe bend, there is a threshold value for the crack angle; further on, it begins to weaken the elbows when subjected to closing bending moment. The proposed solutions included equations normalized with plastic loads of uncracked elbows that have undergone pure in-plane bending [28] and part-through surface-cracked elbows under combined loading of in-plane bending and internal pressure [29,30]. Here again the influences of ovality and thinning on the plastic loads of pipe bends were not considered in the analysis.

The objective of this work is to identify suitable bend cross sections for through-wall circumferential critically cracked 90° pipe bends to include structural deformations in the FE models and investigate the effect of ovality and thinning on the collapse loads (using twice-elastic-slope method) of these cracked pipe bends undergoing combined loading of in-plane closing bending moment and internal pressure. FE analysis was systematically conducted with large geometric change option using elastic–perfectly plastic material. The influences of bend radius and thickness on the plastic loads are also examined.

2. Definitions

2.1. Ovality and thinning

In this study, to account for the nonuniform variation in geometry, two cross sections, namely, elliptic and semioval, are postulated at the bend and analyzed. The required ovality and thickness variation are assumed to vary linearly away from the bend portion. Thus, the cross sections become circular at the two ends of the bend. Fig. 1 shows a schematic representation of ovality along with thinning at extrados and thickening at intrados of the cracked pipe bend model for the two-bend cross sections.

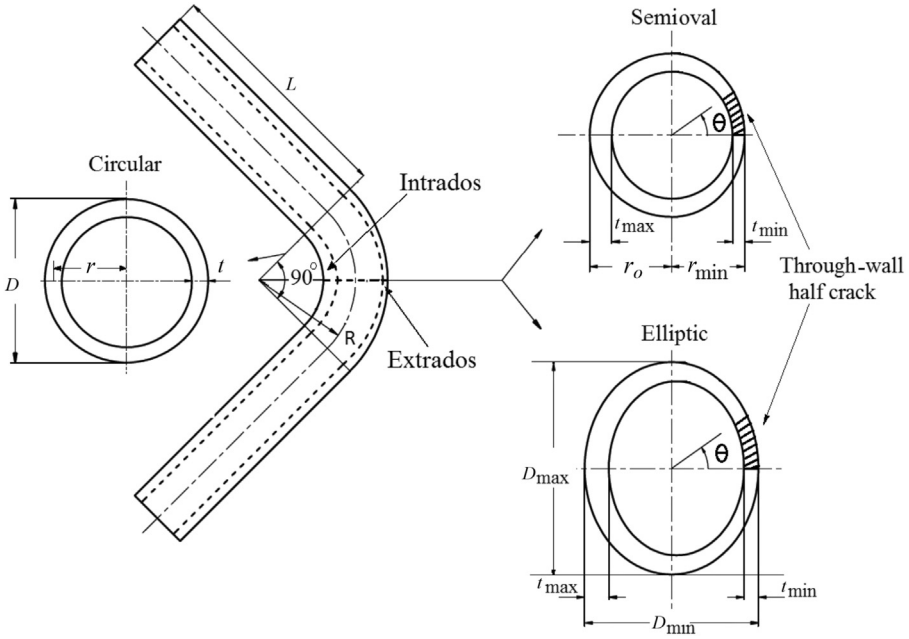

Fig. 1 – Cracked 90° pipe bend with an attached straight pipe showing elliptic and semioval cross sections.

2.1.1. Elliptic cross section

The extent of ovality is calculated by taking the variation between the major and minor diameters and dividing them by the nominal diameter of the pipe [17].

$$\%\text{Ovality},\ C_O = \frac{(D_{max} - D_{min})}{D_O} \times 100 \quad (1)$$

where

$$D_O = (D_{max} + D_{min})/2$$

2.1.2. Semioval cross section

The extent of ovality for semioval cross section is incorporated by taking the variation between the nominal outside and minor radii and dividing by the nominal outside radius of the pipe [19].

$$\%\text{Ovality},\ C_O = \frac{(r_O - r_{min})}{r_O} \times 100 \quad (2)$$

Thinning [19], which appears at extrados of the pipe bend, is described as the ratio of the difference between the nominal thickness and the minimum thickness to the nominal thickness of the pipe bend expressed in percentage as given in the following equation:

$$\%\text{Thinning},\ C_t = \frac{(t - t_{min})}{t} \times 100 \quad (3)$$

$$\text{Bend characteristic},\ \lambda = \frac{\text{Bend ratio}}{\text{Pipe ratio}} = \frac{R/r}{r/t} = \frac{Rt}{r^2} \quad (4)$$

The mean radius and thickness of the pipe are designated as r and t, respectively, and the bend radius as R (see Appendix 1 for definitions of symbols used in this paper).

2.2. Plastic collapse loads

Plastic collapse load or moment is obtained from moment–rotation curves utilizing the twice-elastic-slope method [31] in which a straight line from the origin equal to two times the slope of the elastic region of the moment–rotation curve is drawn to traverse the same curve. The moment–rotation curve for a typical cracked pipe bend model considering nonlinear geometry when loaded with internal pressure is shown in Fig. 2. Plastic instability load is defined as the maximum point in the moment–rotation curves [32].

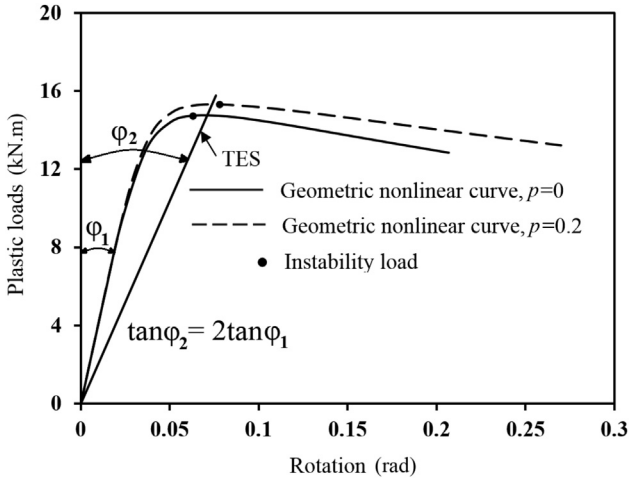

Fig. 2 – Moment–rotation curves for a typical cracked pipe bend (r/t = 5). TES, twice-elastic slope.

3. FE analysis

3.1. Geometry

The FE models considered for the analysis involve 90° pipe bends with critical circumferential through-wall crack at the extrados. Ovality and thinning for the postulated cross sections were each altered from 0% to 20% in steps of 5% [19], to include the acceptable range of distortions in pipe bend standards. Two equal-length straight pipes (L = 5R) are attached tangentially to the pipe bend [27]. The straight pipe attachment eliminates the end effects generated by the boundary conditions. Through-wall circumferential crack has a higher detrimental effect on the collapse moment of elbows compared with other crack configurations [22]. This study therefore considers only through-wall circumferential crack with threshold crack angles. The circumferential through-wall crack is expressed by its relative crack length, θ/π, where θ denotes the half crack angle [28]. Relative crack lengths analogous to threshold crack angles on pipe bends for three different pipe ratios at corresponding normalized pressures p ($Pr/t\sigma_O$) have been considered for pipe bends with circular cross sections [27]. The geometric and material parameters chosen from previous studies were used in this work (Table 1). To evaluate the critical crack angles corresponding to varying degrees of ovality and thinning, the crack angles were changed from the critical crack angle chosen for the corresponding pipe bends with circular cross section. Depending on the weakening or strengthening effect (due to the structural distortions along with loading) on the collapse loads, the critical crack angles can either decrease or increase. The collapse loads thus obtained for the irregular cracked pipe bends with ovality/thinning under external loading were compared with collapse loads for irregular uncracked pipe bends under the same loading conditions.

Let M_{OL} be the collapse load of cracked pipe bend with ovality; M_{Ov} the collapse load of uncracked pipe bend with ovality; M_{TL} the collapse load of cracked pipe bend with thinning; and M_{Th} the collapse load of uncracked pipe bend with thinning.

The crack angle for which M_{OL}/M_{Ov} or M_{TL}/M_{Th} is equal to one is determined (tabulated in Tables 2 and 3) as the critical crack angle for the selected value of ovality or thinning. At and below the critical crack angle, the collapse load of the irregularly cracked pipe bend becomes equal to the collapse load of the irregular uncracked pipe bend. Thus, the irregular cracked pipe bend model behaves like an irregular uncracked pipe bend, as the presence of crack does not have any weakening effect on the collapse load of the pipe bend.

Table 1 – Geometry parameters and material properties for the finite-element model.

Parameter	Specification												References
Geometry													[19,27]
Mean radius of pipe, r	50 mm												
Bend ratios, R/r	2, 3												
Pipe ratios, r/t	5				10				20				
Normalized pressure, ($p = Pr/t\sigma_O$)	00	00.2	00.4	00.6	00	00.2	00.4	00.6	00	00.2	00.4	00.6	
Crack angle (2θ), degree	445	442.5	440	337.5	660	555	550	447.5	990	660	550	445	
Ovality and thinning	0–20% in steps of 5%												
Material	Stainless steel												[28]
Elastic modulus, E	200 GPa												
Poisson's ratio, ν	0.3												
Yield stress, σ_O	200 MPa												

Table 2 – Variation of critical crack angle due to thinning for through-wall circumferential crack pipe bends under in-plane closing bending.

Sample No.	r/t	Normalized pressure	R/r	Critical crack angle for various thinning (°)				
				0	5	10	15	20
1	5	0	2	45	44.85	44.7	44.6	44.5
2			3	45	44.75	44.5	44.25	44
3		0.2	2	42.5	42.35	42.1	41.85	41.75
4			3	42.5	42.25	42	41.75	41.5
5		0.4	2	40	39.85	39.75	39.65	39.5
6			3	40	39.8	39.7	39.5	39.45

3.2. *Meshing*

The FE modeling and analysis were conducted using a standard nonlinear FE package [33]. For the analysis, a coding language was used to write a program for the cracked pipe bends with the chosen cross sections and geometric parameters subjected to internal pressure and in-plane closing moment loading. The material model was presumed to be elastic–perfectly plastic, and nonhardening J2 flow theory was used. The FE model for the crack tip was formed with

Table 3 – Variation of critical crack angle due to ovality for through-wall circumferential crack pipe bends under in-plane closing bending.

Sample No.	r/t	Normalized pressure	R/r	Critical crack angle for various ovality (°).				
				0	5	10	15	20
1	5	0	2	45	43.75	42.5	41.25	40
2			3	45	44.25	43.5	42.75	42
3		0.2	2	42.5	41.5	40.5	39.5	38.5
4			3	42.5	42	41.5	41	40.5
5		0.4	2	40	39.5	39.25	39	38.5
6			3	40	39.75	39.5	39.25	39
7		0.6	2	37.5	38	38.5	39	39.5
8			3	37.5	37.75	38.25	38.5	39
9	10	0	2	60	59	57.75	56.5	55.5
10			3	60	58.75	57.5	56.25	55
11		0.2	2	55	53.5	52.25	50.75	49.5
12			3	55	53.75	52.75	51.5	50.5
13		0.4	2	50	51.5	53.25	54.75	56.5
14			3	50	51.25	52.75	54.25	55.5
15		0.6	2	47.5	48.75	50	51.25	52.5
17			3	47.5	50	52.5	55	57.5
18	20	0	2	90	83.75	77.5	71.25	65
19			3	90	82.5	75	67.5	60
20		0.2	2	60	54	49	43	38
21			3	60	56	51	46	42
22		0.4	2	50	45	41	36	32
23			3	50	55	60	65	70
24		0.6	2	45	49	52	56	60
25			3	45	50	55	60	65

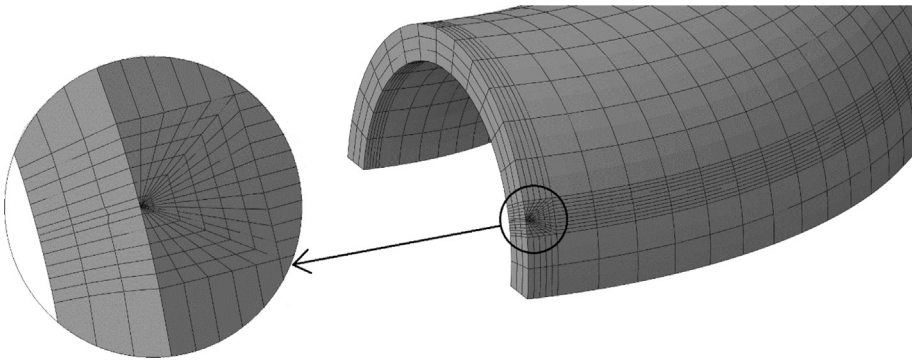

Fig. 3 – A section of the finite-element model with meshes around the crack tip of circumferential through-wall crack at the extrados.

collapsed elements, and a ring of wedge-shaped elements was used in the crack-tip region. Fig. 3 shows a section of the FE meshed model with radial and circumferential divisions employed for the spider web mesh around the crack tip. Mapped meshing was utilized to mesh the cracked pipe bend models so that the number of elements could be controlled. The chosen element type was C3D20R, 20-node isoparametric quadratic brick, reduced integration element. Mesh

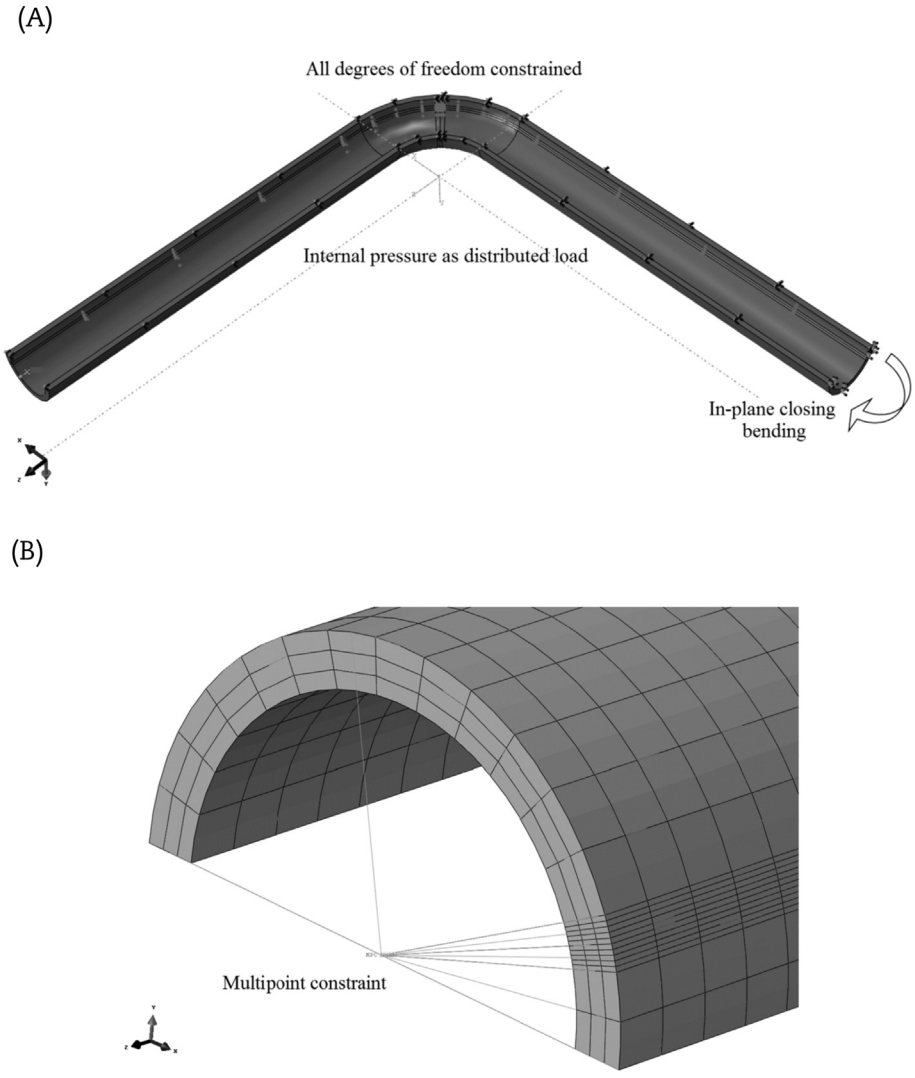

Fig. 4 – (A) Boundary and loading conditions for the finite-element model with half symmetry. (B) End nodes of cracked pipe bend model constrained.

refinement for the models was performed by changing the number of elements across the thickness from 1 to 5. The total number of elements across the model was varied as 6,580, 9,160, 9,945, 13,310, 14,220, and 19,280. The optimum minimum number of elements was chosen as 9,945 for bend ratio 2 and 14,220 for bend ratio 3, because the variation in calculated moments was within 1%. For all the models, the number of elements across the thickness was thus chosen to be three.

3.3. *Boundary and loading conditions*

One half of the cracked pipe bend model, which is symmetric about the longitudinal axis, as shown in Fig. 4A, was built and symmetric boundary conditions were applied. The load is apportioned into two parts: a constant internal pressure applied initially followed by in-plane closing bending moment monotonically increasing in specific steps. This kind of non-proportional loading condition closely simulates the actual operating conditions. All viable degrees of freedom at one end portion of the straight pipe were restrained and multipoint constraint, as shown in Fig. 4B, was affected to the other end wherein the end surface nodes were anchored to a single node for which the rotation boundary condition was defined. Closing in-plane bending is considered as only this type of bending mode opens the crack located at the extrados. Internal pressure was introduced at the inner surface of the models as a distributed load together with an axial tension equivalent to the internal pressure at the end of the pipe to simulate closed end. The RIKS option available within the package was used to overcome problems linked to convergence in elastic–perfectly plastic computations. The input files were generated separately for each model and data were collected for solving the models. The reaction moments proportionate to the stipulated rotations at the multipoint constraint node were extracted directly into Excel sheets. The curves were plotted using the moment and rotation input details.

3.4. *Validation of analysis*

To confirm the reliability of the present FE limit analysis, the collapse moments obtained were verified with the published collapse moment solutions [25,27] as given in Eq. (5) for through-wall circumferentially cracked pipe bends with circular cross sections undergoing combined in-plane bending and internal pressure loading.

$$M_L = M_O X \tag{5}$$

where $M_O = 4r^2 t\sigma_y\left[1.075\lambda^{2/3} + \frac{2.071p^{1.418}}{\lambda^{0.228}} + 8.41p^{12.129}\right][1-p]$and

$$X = 1.1194 - 0.7236\left(\frac{\theta}{\pi}\right) - 2.0806\left(\frac{\theta}{\pi}\right)^2 - 3.4164p^{0.8408}\left(\frac{\theta}{\pi}\right)^{2.1758} \quad \text{for } r/t = 5, \tag{6}$$

$$X = 1.6039 - 1.0847\left(\frac{\theta}{\pi}\right)^{0.4082} - 3.1773p^{0.4807}\left(\frac{\theta}{\pi}\right)^{1.4381} \quad \text{for } r/t = 10, \tag{7}$$

$$X = 7.7803 - 6.8959\left(\frac{\theta}{\pi}\right)^{0.0231} - 4.1061p^{0.5464}\left(\frac{\theta}{\pi}\right)^{1.2776} \quad \text{for } r/t = 20 \tag{8}$$

Under pure in-plane bending moment, the collapse moments were evaluated by putting $p = 0$ for Eqs. (5)–(8). As shown in Fig. 5, the average difference in collapse moments (for $r/t = 20$) between Eq. (5) and FE for normalized pressure from 0 to 0.6 is 3.26%. Similarly, the average difference in collapse moments for $r/t = 10$ for the various pressures is 3.24%. The comparison of FE results and Eq. (5) showed good agreement with an average difference of 4.15% for $r/t = 5$. Thus, the present FE limit analysis procedure was validated.

4. Interpretation of results

4.1. *Comparison between elliptic and semioval cross sections*

To study the influence of ovality and thinning on collapse loads of cracked pipe bends under combined loading, the reference (with circular cross sections) and irregular models (with varying degrees of ovality and thinning) were compared by calculating the percent difference given by

$$Z = \frac{M_R - M_I}{M_R} \times 100 \tag{9}$$

where M_R and M_I are the collapse loads of the reference and irregular models (with elliptic/semioval cross sections), respectively. Based on the comparative evaluation, suitable cross section from the two postulated cross sections is chosen.

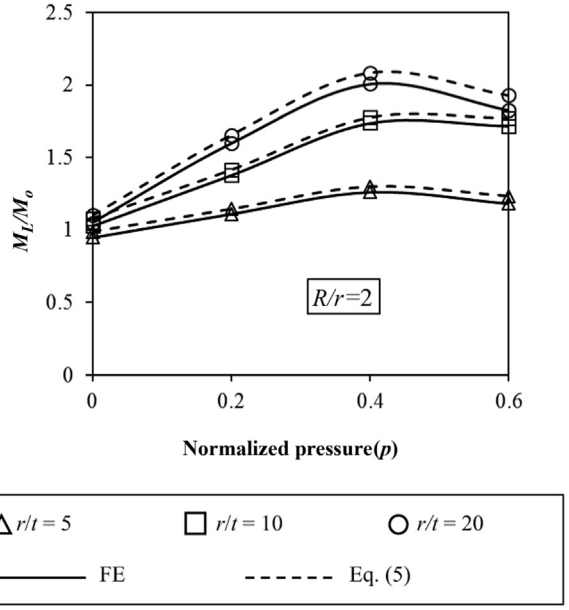

Fig. 5 – Comparison of finite element (FE) collapse moment with Eq. (5).

4.2. *Effect of thinning on collapse moments*

The effects of thinning on collapse loads of cracked pipe bends with elliptic and semioval cross sections are shown in Figs. 6A–6D. The percent difference of collapse loads is computed for combined loading of moment and pressure ($p = 0.2$ and $p = 0.4$) for $r/t = 5$ at bend ratios 2 and 3. From the figures, it is evident that the effect of thinning is minimal for any ovality, although between cross sections, elliptic cross sections show higher percent difference at higher values of ovality. The maximum percent difference due to thinning for elliptic cross section at $p = 0.2$ was 1.53% as shown in Fig. 6B. At $p = 0.4$, the maximum percent difference due to thinning was 0.97%, which occurred again for elliptic cross section as in Fig. 6D. The same trend was observed for pipe ratios 10 and 20 with the associated crack geometries.

4.3. *Effect of ovality on collapse moments*

The influence of ovality on collapse loads of cracked pipe bends with the postulated cross sections can be observed in Figs. 7A–7F. Positive values of percent difference indicate that ovality should be considered in the analysis of cracked pipe bends because the magnitude of collapse loads for the irregular models is less than that of the reference models. For $r/t = 10$ and $r/t = 20$, at $p = 0.4$, the negative percent difference (associated with the increase of stiffening effect due to internal pressure) for semioval cross sections is less when compared with elliptic cross sections. As shown in Fig. 7F, at 20% ovality, the maximum negative percent difference of 8.9% is seen for elliptic cross section for pipe ratio 20, at $p = 0.4$. Hence, semioval cross sections are preferred for cracked pipe bend models with a pipe ratio 20. The positive percent difference is seen for elliptic cross sections with $r/t = 5$ (at $p = 0.2$ and $p = 0.4$) and $r/t = 10$ (at $p = 0.2$). For pipe ratio 5, the maximum positive percent difference of 7.1% (Fig. 7A) and 3.6% (Fig. 7B) is seen for elliptic cross sections at normalized pressures of 0.2 and 0.4, respectively. Therefore, elliptic cross section is conducive for analysis of cracked pipe bends with $r/t = 5$ and $r/t = 10$ (at $p = 0.2$). For pipe ratio 10, at $p = 0.4$, the negative percent difference is higher for semioval cross sections with bend ratio 2 (Fig. 7D), whereas with bend ratio 3,

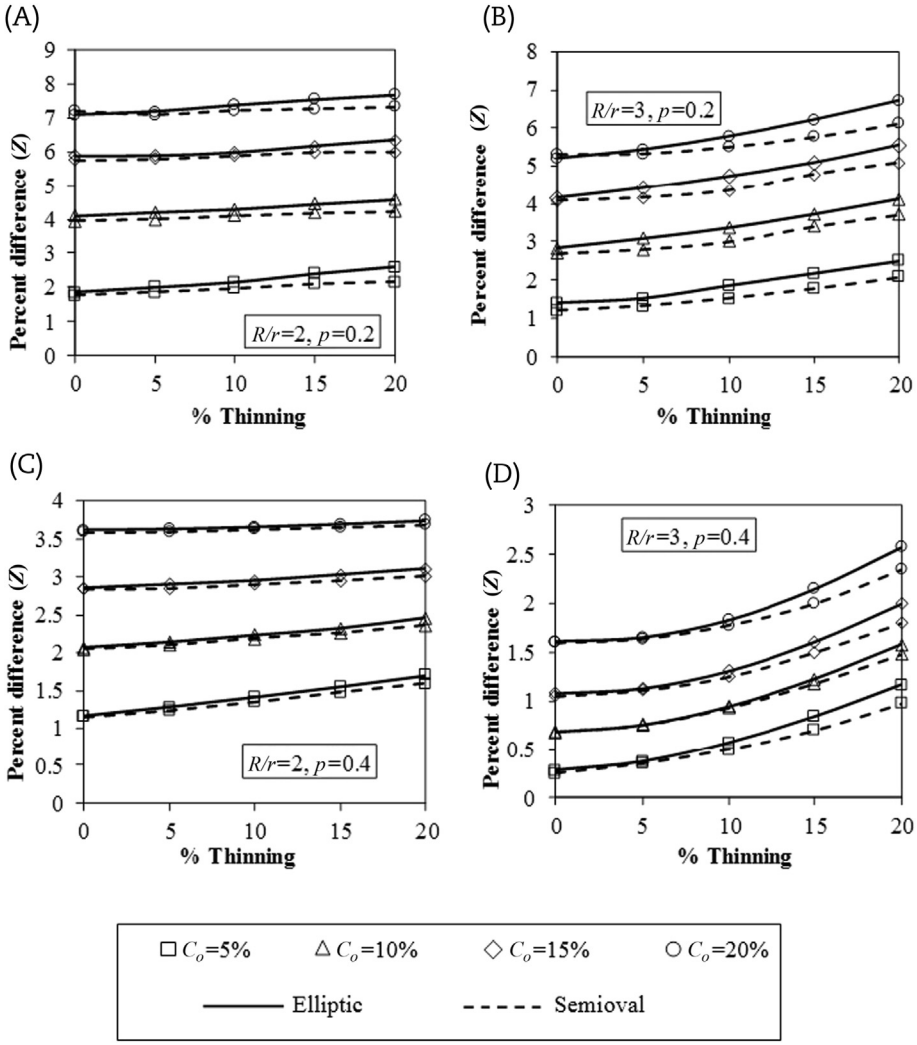

Fig. 6 – Combined effect of ovality and thinning on collapse loads of cracked pipe bends with elliptic and semioval cross sections for $r/t = 5$.

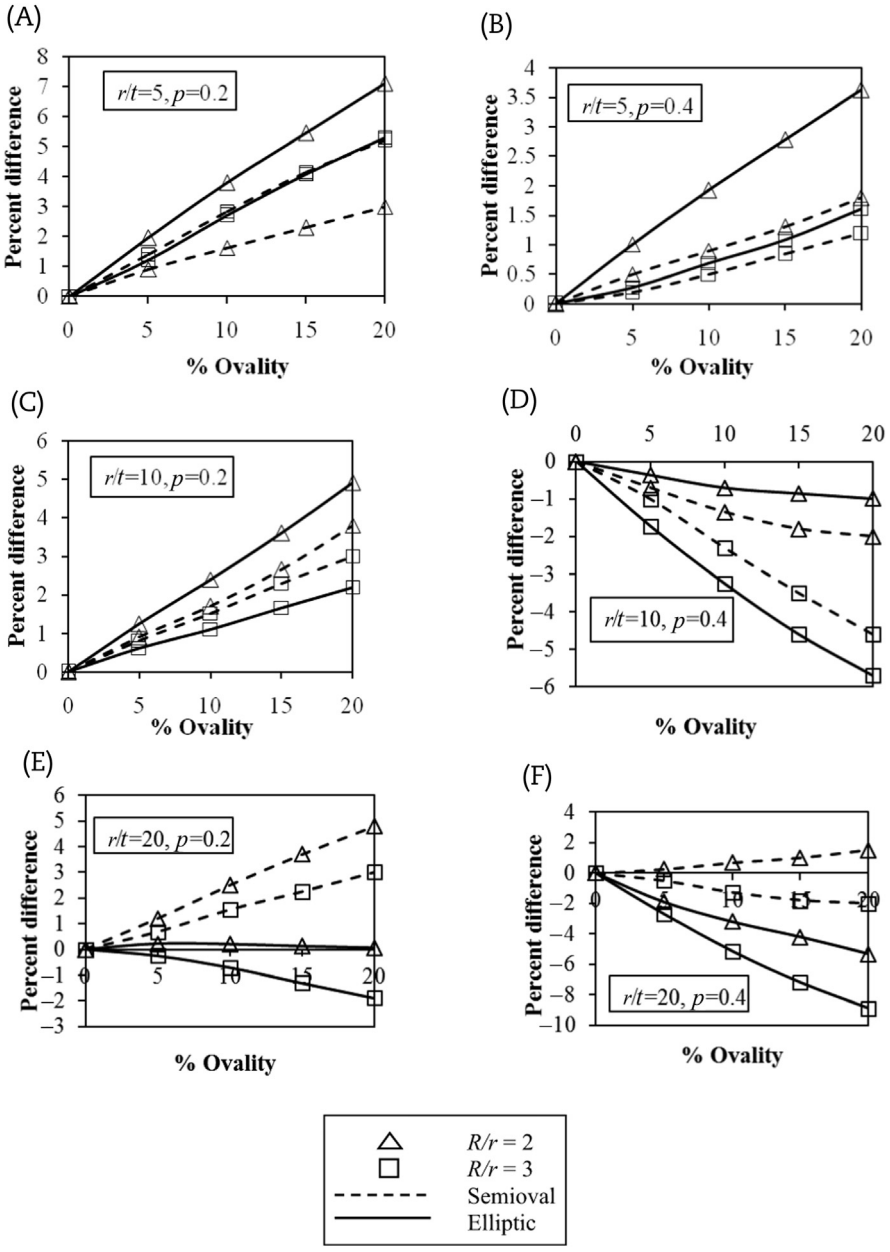

Fig. 7 – Effect of ovality on plastic loads of cracked pipe bends under combined loading for various *R/r* and *r/t*.

elliptic cross sections have a higher negative percent difference. Thus, both cross sections can be assumed for pipe ratio 10 at $p = 0.4$. When internal pressure is applied along with an in-plane closing bending moment, the weakening effect produced by the bending moment is counteracted by the internal pressure and bending stiffness is increased [9]. Therefore, the negative percent difference in collapse loads is due to the influence of ovality on internal pressure and the positive value is credited to the decrease of the stiffening effect.

4.4. *Effect of thickness and bend radius*

The collapse loads calculated for the irregular models under combined loading are given in Figs. 8A–8D. From the figures, it is observed that the collapse loads increase with increase in thickness and bend radius. The effect of ovality on the collapse moments has a distinct influence on cracked pipe bend models with pipe ratio 5 when compared with the other two pipe ratios. With increase in pressure, the difference between collapse loads for FE models with bend ratios 2 and 3 decreases with increase in ovality. The decrease in collapse loads with increase in ovality showed a marked declining trend for all models with elliptic cross sections when matched with semioval cross sections.

4.5. *Effect of internal pressure*

Based on the results of the comparison of postulated cross sections, elliptical cross sections were chosen to model the cracked pipe bend models with pipe ratios 5 and 10, whereas

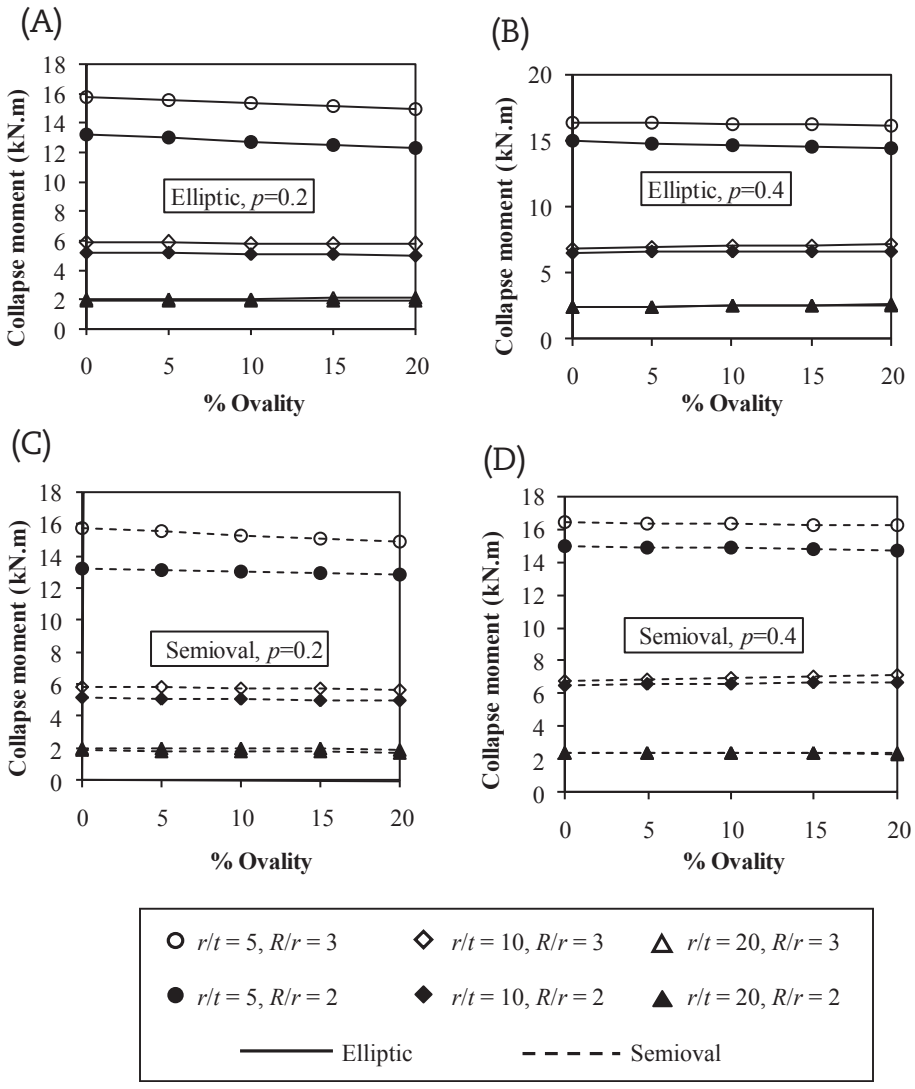

Fig. 8 – Variation of collapse moments with ovality for cracked pipe bends with elliptic and semioval cross sections under combined loading.

semioval cross sections were used for cracked pipe bend models with pipe ratio 20. The results of the study are presented in Figs. 9–11. Under pure in-plane closing bending moment (when $p = 0$), the geometry of the cracked pipe bend weakens due to ovalization of the cross section. The presence of ovality weakens the cracked pipe bends as the collapse loads are below the reference models. The positive percent difference in collapse moments is maximum, as shown in Figs. 9–11, for all ovalities under moment load alone. When the cracked pipe bend is subjected to combined moment and pressure loading, the internal pressure counteracts against the ovalization of the bend cross section and attempts to maintain the cross section circular. This stiffening effect also increases the collapse load. It is also observed that under combined moment and pressure loading, the collapse loads decrease below the reference model due to the influence of ovality for low pressures. As pressure increases, the effect of ovality reduces and for a particular value of pressure, this effect is more or less cancelled out as the percent difference for all ovality values is nearly equal and closer to zero. The negative percent difference increases as the internal pressure increases further, which shows that the presence of ovality raises the stiffness of the pipe bends for higher pressures. Hence, it can be inferred that for pure in-plane closing moment loading, augmentation of ovality increases the percent difference between collapse loads for all the cracked pipe bend models considered. When the pressure load is also applied, this trend continues up to a particular pressure, beyond which the increase in ovality causes a positive effect of increasing the collapse load.

For r/t = 20, at R/r = 2, under pure in-plane closing moment loading (without internal pressure), the positive percent difference is 2.2%, 4.4%, 6.5%, and 8.6%, respectively, for the ovality of 5%, 10%, 15%, and 20%, as shown in Fig. 9A, which indicates that the presence of ovality weakens the bend geometry. When the internal pressure is applied, the weakening effect of ovality on collapse loads diminishes and this invalidating pressure occurs between 0.4 and 0.6 MPa for bend

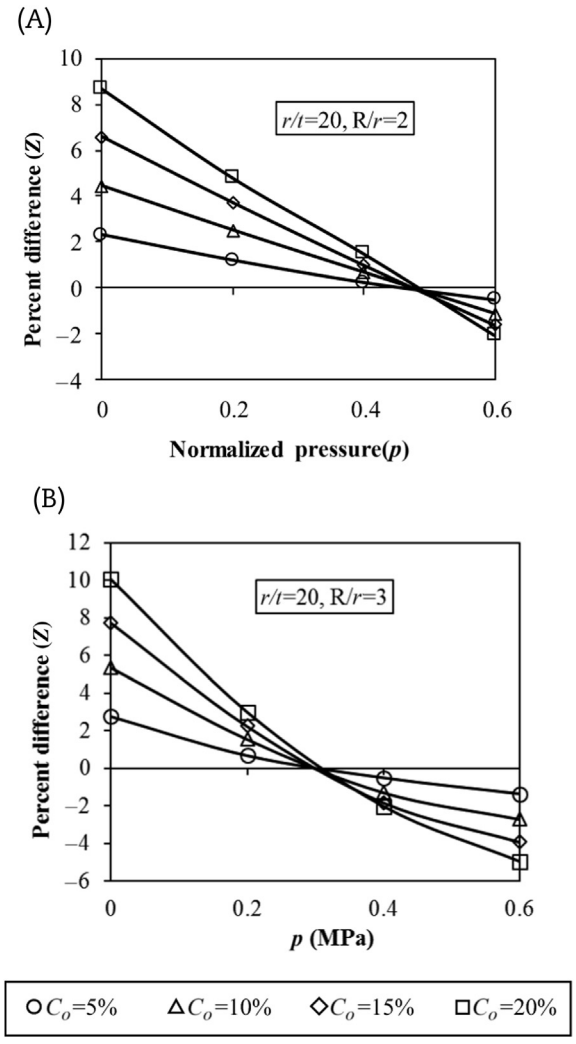

Fig. 9 – Effect of internal pressure and ovality on collapse loads for r/t = 20.

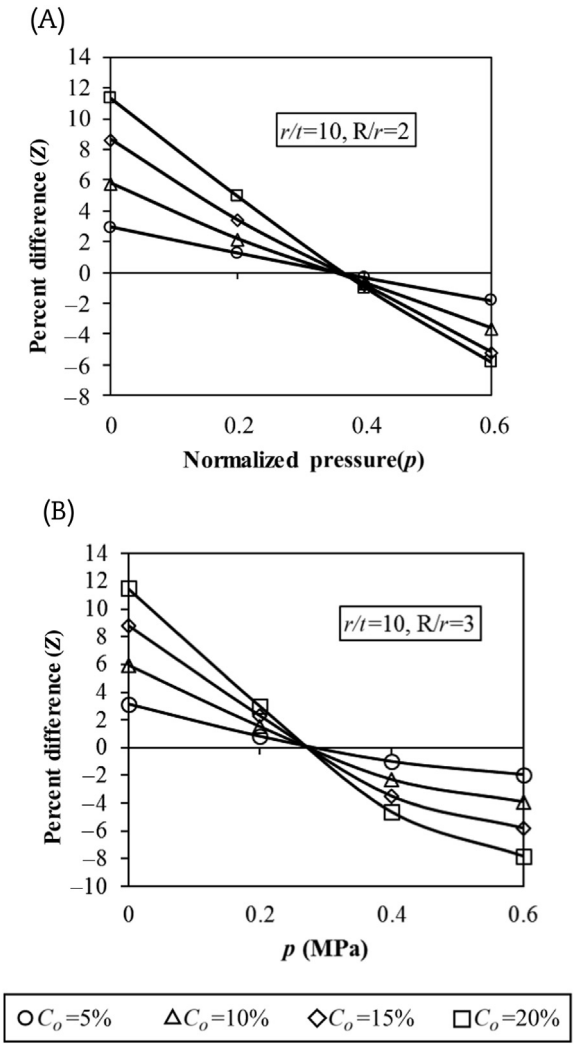

Fig. 10 – Effect of internal pressure and ovality on collapse loads for r/t = 10.

ratio 2 (Fig. 9A). At the invalidating pressure, the stiffness of the bend is unchanged by ovality, implying that this pressure is adequate enough to surpass the effect of ovality and the cracked pipe bend acts like the one with circular cross section. For bend ratio 2, when the pressure is 0.6, the percent differences are −0.5%, −1.1%, −1.6%, and −2.0%, respectively, for the ovality of 5%, 10%, 15%, and 20%. A similar trend is observed for r/t = 20, R/r = 3 with the invalidating pressure occurring between 0.2 and 0.4 MPa (Fig. 9B). For pure in-plane closing moment loading, the percent difference for ovality of 5%, 10%, 15%, and 20% is 2.7%, 5.3%, 7.7%, and 10%, respectively, for the bend radius of 150 mm, as shown in Fig. 9B. For the maximum applied internal pressure of 0.4 MPa, the difference is −0.5%, −1.2%, −1.8%, and −2% for the corresponding ovalities.

The findings presented in Figs. 10 and 11, for r/t = 10 and 5 with the chosen bend ratios and the associated crack parameters are similar to r/t = 20, which has been discussed in previous sections. The invalidating pressure for pipe ratio 5 is between 0.4 and 0.6 MPa, whereas for pipe ratio 10, it falls between 0.2 and 0.4 MPa. Increase in thickness of pipe bend increases the invalidating pressure. Because the pressure range selected for this study is to study the effect of ovality on the collapse moment of cracked pipe bends, for some of the cases considered, as shown in Figs. 9 and 10, the pressure was not varied beyond $p = 0.4$, since the invalidating pressure occurred earlier. The invalidating pressures indicate that, at and above the invalidating pressure, the presence of ovality improves the performance of cracked pipe bends and increase in ovality further enhances it. Because thinning does not produce any significant effects, ovality and thinning limits for estimation of collapse loads of cracked pipe bends need not be emphasized at and beyond the invalidating pressure.

5. Comparison with experimental results

Validation of the analysis of a physical phenomenon (e.g., collapse moments) by comparing it with experimental results assures that the predictions are in agreement with reported observations. Therefore, efforts have been made to compare

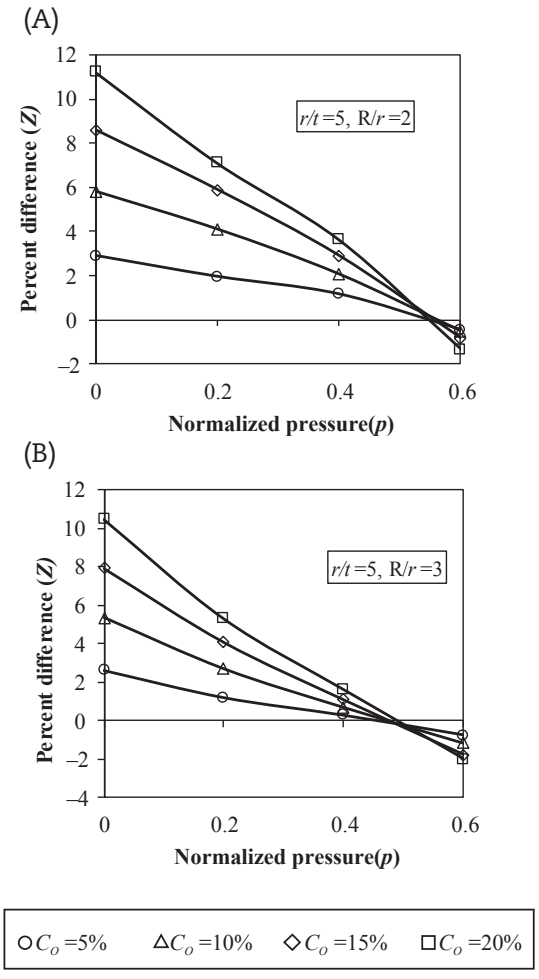

Fig. 11 – Effect of internal pressure and ovality on collapse loads for r/t = 5.

the predictions of the FE analysis with available experimental results and to rationally describe the behavior.

For the unpressurized case, the geometry and parameters of the cracked pipe bend reported in experimental data [25] were input into the FE model. The predicted collapse moments obtained from the FE models with varying degrees of ovality were compared with experimental results. As shown in Table 4, for the pipe bend with circumferential through-wall crack at the extrados, at 0% ovality, a difference of 7.58% exists between the experimental and FE collapse moment results. This percent difference increases to 17.98 as ovality reaches 20%. Although the degree of ovality in the experimental pipe bend was not mentioned, it could be presumed that there remained some percentage of ovality. Moreover, the percentage difference is higher, as this analysis assumed the cracked pipe bend material to be elastic–perfectly plastic without considering strain hardening effects associated with bending.

Under combined loading of internal pressure and bending moment, no experimental data are available in the published studies for comparison with FE results. Therefore, reasonable explanations are presented in the "Effect of ovality on collapse moments," "Effect of thickness and bend radius," and "Effect of internal pressure" sections in support of the findings reported in the present analysis.

6. Conclusions

The influence of structural deformations (ovality and thinning) on the collapse loads of through-wall circumferential critically cracked 90° pipe bends undergoing in-plane bending and internal pressure was investigated using FE analysis based on elastic–perfectly plastic material with large geometric change effect. To incorporate ovality and thinning, two cross sections, namely, elliptic and semioval, were postulated at the bend and compared for their suitability in analysis. The conclusions drawn based on the analyses conducted are as follows:

Postulated cross sections: Under combined in-plane closing bending moment and internal pressure, the presence of ovality in critically cracked pipe bends increases the magnitude of the collapse loads beyond the reference models for elliptic cross sections with $r/t = 20$ with both bend radii. The same has been observed for both cross sections with $r/t = 10$ ($p = 0.4$), with the negative percent difference increasing with increase in bend radius. For other models considered, the collapse load decreases with respect to the reference models. Thus, with increase in pipe ratio, at higher values of internal pressure, semioval cross sections may be assumed to account for ovality in the determination of collapse loads of pipe bends with the crack geometries considered subjected to in-plane closing bending. The effect of thinning on collapse loads is minimal for cracked pipe bends with both cross sections when subjected to combined bending and internal pressure, and therefore, thinning need not be considered for analysis.

Table 4 – Comparison between FE and experimental results.

Reference	R, mm	Bend ratio (R/r)	Pipe ratio (r/t)	2θ, degree	% Ovality	Collapse moment (kN·m)		
						Experimental results	FE results	% Difference
Chattopadhyay et al. [25]	207	2.07	5.17	98	0	108.7	100.45	7.58
					5		97.62	10.19
					10		94.59	12.98
					15		91.95	15.40
					20		89.15	17.98

% Difference = [(Experiment- FE)/Experiment] × 100.
FE, finite element.

Internal pressure: For each cracked pipe bend model, the presence of ovality decreases the collapse loads of cracked pipe bends below those of the reference model up to a certain value of applied pressure. Beyond this value of applied pressure, the collapse loads of irregular models become higher than those of reference models and this increase in collapse load is related to the increase of stiffness. This invalidating pressure vary with change in thickness and bend radius of cracked pipe bend. At and beyond the invalidating pressure, ovality need not be underscored in analysis of collapse loads of cracked pipe bend models examined.

Conflicts of interest

All the authors have no conflicts of interest to declare.

Acknowledgments

The authors are grateful to the Director, National Institute of Technology (NIT), Tiruchirappalli for his continual encouragement and support for this work. The authors abundantly thank the Computer Support Group (CSG), NIT Trichy, for its support to this work.

Appendix 1. Nomenclature.

The following symbols are used in this paper:

C_O	percent ovality
C_t	percent thinning
D	pipe outside (nominal) diameter, mm
D_{max}	maximum outside pipe diameter, mm
D_{min}	minimum outside pipe diameter, mm
E	Young's modulus, GPa
L	length of straight pipe attached, mm
M_I	collapse moment of cracked pipe bend with irregular cross section, kN·m
M_L	collapse moment of cracked pipe bend under combined internal pressure and in-plane closing bending, kN·m
M_O	collapse moment of uncracked pipe bend under combined internal pressure and in-plane closing bending, kN·m
M_R	collapse moment of cracked pipe bend with circular cross section, kN·m
P	internal pressure, MPa
p	$= Pr/(t\sigma_O)$, normalized internal pressure
R	bend radius to neutral axis, mm
r	mean pipe radius, mm
r_{min}	minimum outside radius at bend section of the semioval cross section, mm
r_o	nominal outside radius of the pipe, mm
t	nominal thickness of pipe bend, mm
t_{max}	maximum pipe thickness, mm
t_{min}	minimum pipe thickness, mm
θ	half crack angle for circumferential through-wall crack
θ	semicircumferential crack angle
θ/π	relative crack length
λ	bend characteristic
σ_O	yield stress of an elastic–perfectly plastic material, MPa

REFERENCES

[1] J. Spence, G.E. Findlay, Limit load for elbows under in-plane bending, in: Proceedings of Second International Conference on Pressure Vessel Technology, vol. 28, 1973, pp. 393–399. San Antonio, TX.
[2] C.R. Calladine, Limit analysis of curved tubes, J. Mech. Sci. 16 (1974) 85–87.
[3] I.W. Goodall, reportLower bound limit analysis of curved tubes loaded by combined internal pressure and in-plane bending moment, CEGB Rep. No. RD/B/N4360, Central Electricity Generating Board, London.
[4] S.E. Bolt, W.L. Greenstreet, reportExperimental determination of plastic collapse loads for pipe elbows, ASME Rep. No. 71-PVP-37, ASME, New York.
[5] J.E. Griffiths, The effect of cracks on the limit load of pipe bends under in-plane bending—experimental study, Int. J. Mech. Sci. 21 (1979) 119–130.
[6] W.L. Greenstreet, Experimental study of plastic responses of pipe elbows, Rep. No. ORNL/NUREG-24, 1–51.
[7] P. Hilsenkopf, B. Boneh, P. Sollogoub, Experimental study of behavior and functional capability of ferric steel elbows and austenitic stainless steel thin walled elbows, Int. J. Press. Vessel Piping 33 (1998) 111–128.
[8] T. Hassan, M. Modlin, V.C. Matzen, in: Data Developed at the Center for Nuclear Power Plant Structures, Equipment and Piping, North Carolina State University, Raleigh (NC), 2000.
[9] K. Wilkins, Y. Tan, V.C. Matzen, Data Developed at the Center for Nuclear Power Plant Structures, Equipment and Piping, North Carolina State University, Raleigh (NC), 2001.
[10] K. Wilkins, Experimental and analytical investigation into the non-linear behavior of 200 and 400, 90degree large radius, schedule 10, stainless steel elbows under monotonic, cyclic and rate dependent loading, PhD dissertation, North Carolina State University, Raleigh (NC), 2002.
[11] M.A. Shalaby, M.Y.A. Younan, Limit loads for pipe elbows with internal pressure under in-plane closing bending moments, J. Press. Vessel Tech. 120 (1998) 35–42.
[12] J. Chattopadhyay, D.K. Natahani, B.K. Dutta, H.S. Kushwaha, Closed-form collapse moment equations of elbows under internal pressure and in-plane bending moment, J. Press. Vessel Tech. 122 (2000) 431–436.
[13] A. Robertson, H. Li, D. Mackenzie, Plastic collapse of pipe bends under combined internal pressure and in-plane bending, Int. J. Press. Vessel Piping 82 (2005) 407–416.
[14] Y.J. Kim, C.S. Oh, Limit loads for elbows under combined pressure and in-plane bending based on finite element limit analysis, Int. J. Press. Vessel Piping 83 (2006) 85–90.
[15] Y.J. Kim, C.S. Oh, Closed-form plastic collapse loads of pipe bends under combined pressure and in-plane bending, Eng. Fract. Mech. 73 (2006) 1437–1454.
[16] L. Xuming, L. Shilei, H. Zhang, Y. Wang, Z. Wang, F. Xue, X. Wang, Leak-before-break analysis of thermally aged nuclear pipe under different bending moments, Nucl. Eng. Technol. 47 (2015) 712–718.

[17] A.R. Veerappan, S. Shanmugam, Analysis for flexibility in the ovality and thinning limits of pipe bends, ARPN J. Eng. Appl. Sci. 3 (2008) 31–41.
[18] A.R. Veerappan, S. Shanmugam, S. Soundrapandian, The accepting of pipe bends with ovality and thinning using finite element method, J. Press. Vessel Tech. 132 (2010) 1–4.
[19] T. Christo Michael, A.R. Veerappan, S. Shanmugam, Comparison of plastic limit and collapse loads in pipe bends with shape imperfections under in-plane bending and internal pressure, Int. J. Press. Vessel Piping 99–100 (2012) 23–33.
[20] V. Dan, The influence of the initial ovality tolerance on the non-linear cycling analysis of piping bends, J. Press. Vessel Tech. 131 (2009) 1–7.
[21] Y.J. Kim, N.H. Kim, C.Y. Oh, C.S. Oh, A method to estimate plastic loads for elbows with non-uniform thicknesses, Fatigue Fract. Eng. Mater. Struct. 31 (2008) 822–837.
[22] A.G. Miller, Review of limit loads of structures containing defects, Int. J. Press. Vessel Piping 32 (1998) 291–327.
[23] J.H. Park, Y. Ki, C. Sun, H. Kim, J.H. Lee, Estimation of leak rate through circumferential cracks in pipes in nuclear power plants, Nucl. Eng. Technol. 47 (2015) 332–339.
[24] K. Yahiaoui, J. Chattopadhyay, B.K. Dutta, H.S. Kushwaha, Experimental and analytical study of three point bend specimen and throughwall circumferentially cracked straight pipe, Int. J. Press. Vessel Piping 77 (2000) 455–471.
[25] J. Chattopadhyay, A.K.S. Tomar, B.K. Dutta, Closed-form collapse moment equations of throughwall circumferentially cracked elbows subjected to in-plane bending moment, J. Press. Vessel Tech. 126 (2004) 307–317.
[26] J. Li, C.Y. Zhou, X.T. Miao, L. Chang, X.H. He, Plastic limit loads for pipe bends with circumferential through-wall crack under torsion moment, Int. J. Mech. Sci. 100 (2015) 283–297.
[27] J. Chattopadhyay, A.K.S. Tomar, New plastic collapse moment equations of defect-free and throughwall circumferentially cracked elbows subjected to combined internal pressure and in-plane bending moment, Eng. Fract. Mech. 73 (2006) 829–854.
[28] Y.J. Kim, Y.I. Kim, T.K. Song, Finite element plastic loads for circumferential cracked elbows under in-plane bending, Eng. Fract. Mech. 74 (2007) 643–668.
[29] S.P. Hong, J.H. Kim, Y.J. Kim, P.J. Budden, Effect of internal pressure on plastic loads of 90° elbows with circumferential part-through surface cracks under in-plane bending, Eng. Fract. Mech. 77 (2010) 577–596.
[30] N.H. Kim, C.S. Oh, Y.J. Kim, J.S. Kim, D.W. Jerng, P.J. Budden, Limit loads and fracture mechanics parameters for thick-walled pipes, Int. J. Press. Vessel. Piping 88 (2011) 403–414.
[31] American Society of Mechanical Engineers, ASME Boiler and Pressure Vessel Code, Section III, Nuclear Power Plant Components, Division 1, American Society of Mechanical Engineers, New York, 2000.
[32] American Society of Mechanical Engineers, ASME Boiler and Pressure Vessel Code, Section II, Materials Part A: Ferrous Material Specifications, vol. I, American Society of Mechanical Engineers, New York, 2010.
[33] SIMULIA Corporation, ABAQUS Version 6.10, User's Manual, SIMULIA, Providence (RI), 2010.